



UNIVERSITY OF LEEDS

This is a repository copy of *Failure analysis of the piston used in a pneumatic down the hole impactor*.

White Rose Research Online URL for this paper:
<https://eprints.whiterose.ac.uk/177444/>

Version: Accepted Version

Article:

Wang, J, Han, B, Wang, C orcid.org/0000-0002-4301-3974 et al. (4 more authors) (2021)
Failure analysis of the piston used in a pneumatic down the hole impactor. *Engineering Failure Analysis*, 127. 105561. ISSN 1350-6307

<https://doi.org/10.1016/j.engfailanal.2021.105561>

© 2021, Elsevier. This manuscript version is made available under the CC-BY-NC-ND 4.0 license <http://creativecommons.org/licenses/by-nc-nd/4.0/>.

Reuse

This article is distributed under the terms of the Creative Commons Attribution-NonCommercial-NoDerivs (CC BY-NC-ND) licence. This licence only allows you to download this work and share it with others as long as you credit the authors, but you can't change the article in any way or use it commercially. More information and the full terms of the licence here: <https://creativecommons.org/licenses/>

Takedown

If you consider content in White Rose Research Online to be in breach of UK law, please notify us by emailing eprints@whiterose.ac.uk including the URL of the record and the reason for the withdrawal request.



eprints@whiterose.ac.uk
<https://eprints.whiterose.ac.uk/>

Failure Analysis of the Piston Used in a Pneumatic Down the Hole Impactor

Jialin Wang^{a,b}, Bin Han^{a*}, Chun Wang^b, Yajing Gong^b, Yongsheng Li^c, Anne Neville^b, Ardian Morina^{b*}

^a: School of Materials Science and Engineering, China University of Petroleum (East China), Qingdao, 266555

^b: Institute of Functional Surface, School of Mechanical Engineering, University of Leeds, LS2 9JT, United Kingdom

^c: Shandong Tianrui Heavy Industry Company, Weifang, 261000

*Corresponding author: Bin Han, E-mail: hanbin@upc.edu.cn

Ardian Morina, E-mail: a.morina@leeds.ac.uk

Abstract: In this study, the piston's failure mechanism in the pneumatic down the hole (DTH) impactor has been investigated. To study the cause of surface fracture, material microstructure and hardness have been analysed using SEM and nanoindentation as well as the Vickers hardness tester. The stress state of the piston in the impact process was analysed using ABAQUS finite element software. The results show that the carburized layer transits from the acicular martensite to plate martensite from the surface towards inside. In fracture, the acicular martensite is an intergranular fracture, and the plate martensite is a transgranular fracture. According to the finite element simulation results, the maximum Mises stress occurs when the piston strikes the bit at an angle of 0.22° . High von Mises stress makes the carbides, or the defects in the carburized layer, to crack. Meanwhile, in propagating the stress wave at the piston's impact point, a tensile stress of 560 MPa will be generated on the piston's outer edge, which causes the crack in carbide to grow along the radial and axial direction of the piston.

Keywords: Fatigue fracture, Carburizing layer, Cracks, DTH impactor

1 Introduction

Down the hole (DTH) impactor is a kind of drilling tool used in the mining field. It uses high pressure air to push the piston to hit the rotating drill bit. When the DTH impactor is working, the piston impacts the bit with a final speed of 8-12 m/s, and impact frequency of about 20 Hz. Under this level of high-frequency and high-speed impact, the piston's front is subjected to a significant force at the moment of impact, which causes the piston to fracture as shown in Figure 1.

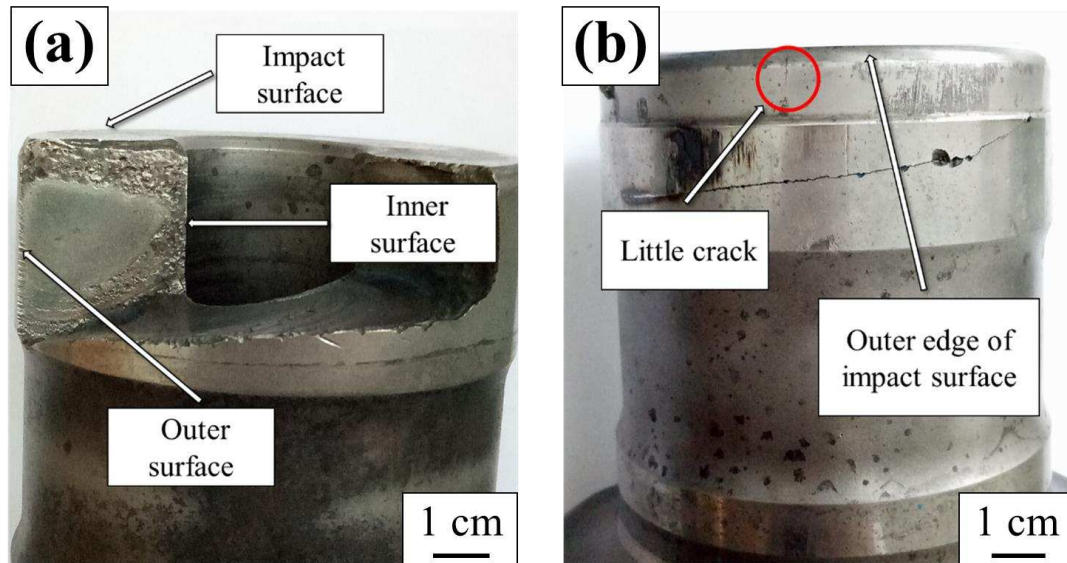


Figure 1 The impact end of the piston, a) The fractured surface, b) The small crack at the outer edge of the piston

It is generally believed that the fracture of rock drilling tools is due to material fatigue because each part of rock drill is subjected to periodic stress when it is in use^[1]. The failure of the rock drill rod was studied before by Abdulbaset et al^[2], where they showed that the crack initiates on the outer surface, then propagates and merges into a large crack during the periodic loading, promoting the crack growth. The piston's fractured surface showed three different regions: crack initiation region, ductile and brittle fracture region, and the final failure region^[2]. For the cause of crack initiation, Tezcan et al.^[1] suggested that piston's crack initiation is caused by the martensitic transformation of retained austenite in a carburized layer during the piston impact, while Abdulbaset et al.^[2] argued that cracks were initiated from the pits. By observing the crack of the failed impact piston, it was found that part of the crack originated from the pits at the outer edge of the impact surface. The cause of this part of the crack can be explained by the mechanism elucidated by Abdulbaset et al.^[2]. However, there is still crack initiation in the impact piston that is not related to the pits, indicating that the cause of the crack initiation of the impact piston may be a result of multiple factors, such as pitting, phase transformation, and inclusions in the piston.

In order to improve the strength and wear resistance of the piston surface, the carburizing-quenching-tempering process is usually used in heat treatment of the piston^[3]. However, many studies have shown that for the carburized steel, fatigue cracks usually originate from the carburized layer on the surface^[4, 5]. In fatigue test of the carburized steel, Farfan et al.^[6] observed that the fracture mode in the carburized layer was intergranular fracture, and that the

fracture mode was similar to that of the rock drill rod. Osman et al. [7] investigated the fatigue fracture and found that the fatigue crack originated in the carburized layer's intergranular fracture region. During the carburizing process, the carburized layer of steel will form carbides such as Fe_3C , $M_{23}C_6$, M_6C and M_7C_3 [8-12]. Kenzo [13] observed that the carbide fracture in the carburized layer is the cause of fatigue crack initiation and that the fatigue life of the material can be improved significantly by volume reduction of primary carbides. For DTH pistons, there is usually a carburized layer of about 2 mm on the surface, and it is subject to a periodic stress during rock drilling. Therefore, the fracture mechanism of rock drilling tools may be the same as that of the carburised steel's fatigue fracture.

The aim of this paper is to investigate the piston of a failed DTH impactor. The cause of microcracks initiation is researched by observing the outer edge of the impact surface of the piston and its cross section. The finite element analysis software was used to solve the Mises stress distribution at the moment when the piston impacts the drill bit. The potential reasons for the crack to occur at the outer edge of the impact face have been explored. Based on Paris' law, the minimum crack length is calculated when the crack $\Delta K > \Delta K_{th}$, and the mode and propagation direction of the fatigue crack have been analysed.

2 Methodology

2.1 Material

The pistons in this study were made of 23CrNi3Mo, and their chemical composition is listed in Table 1. They were carburized at 850 °C for 18 hours, and following carburizing, the pistons were quenched and tempered to improve the strength and hardness. After heat treatment, the tensile strength, yield strength and fatigue strength of the material are 1100 MPa, 800 MPa and 330 MPa respectively. All data about 23CrNi3Mo are provided by the equipment manufacturer. Examples of the failed pistons studied in this paper are shown in Figure 2. The impact end of the piston, shown in Figure 2 (a), has a noticeable crack indicated by the arrow and Figures 2 (b) and (c) show the failure part dropped from the impact end. The pistons in Figure 2 are fractured at the cumulative drilling depth of about 3000 m.

Table 1 Chemical Composition of 23CrNi3Mo in wt%

Element	C	Si	Mn	Cr	Ni	Mo	P	S
Content	0.25	0.2565	0.6455	1.272	2.9285	0.246	0.0105	0.003

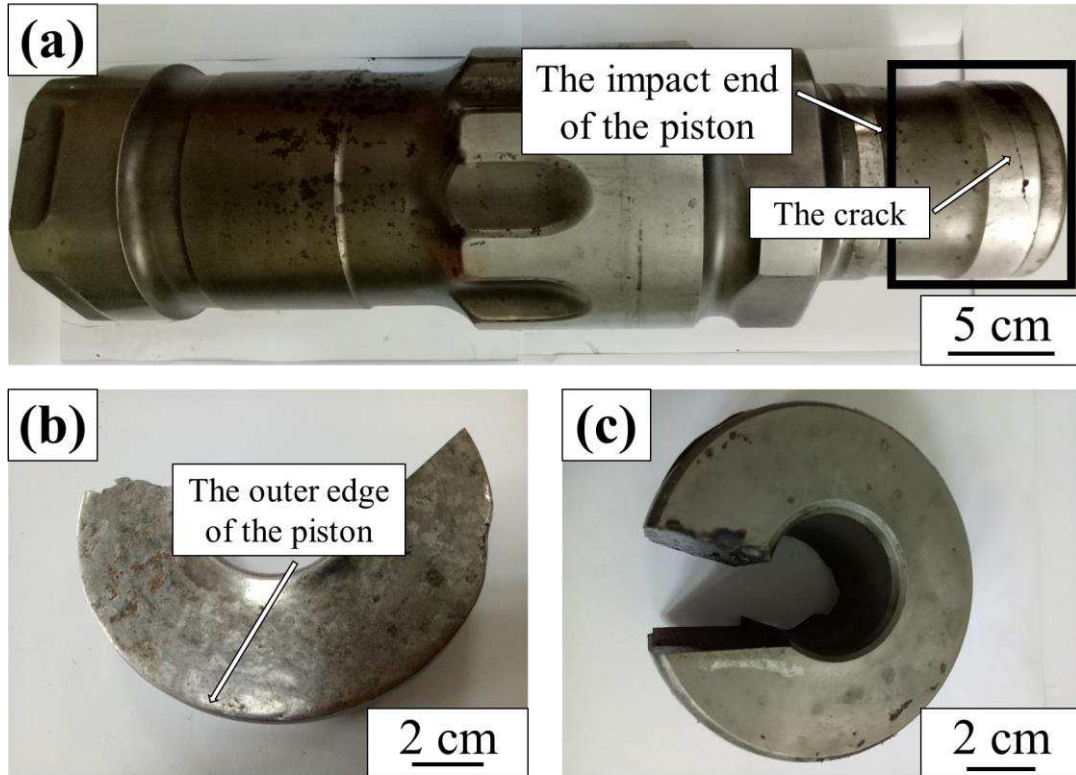


Figure 2 The failure piston of DHT. a) The failure piston with cracks, b) and c) Failure part falling from the impact end of piston

2.2 Experimental methods and simulation

Samples (10 mm×10 mm×20 mm) were cut from the impact surface of the piston using the Wire Electrical Discharge Machine (WEDM). For microstructure analysis, the prepared samples were etched in Nital (2-3% nitric acid in ethanol) solution and examined using a light optical microscope. Hardness gradient measurements were conducted using the Vickers hardness tester and the Nano-indentor. The distribution of carbides in cross-sections of the carburized layer were investigated using the Scanning Electron Microscope (SEM), JEM-7200F, equipped with Oxford EDS system (X-Max50). The fracture surface on the outer edge of each piston was examined using SEM.

Finite element analysis was conducted using ABAQUS to build the simplified piston model and simulate the process of the piston impacting the drill bit. The elastic modulus, Poisson's ratio and density of the material are 2.07×10^5 MPa, 0.3 and 7850 kg/m^3 . The entire piston is divided into 1132975 hexahedral elements by using the C3D8I element (After grid independence analysis, the number of grids is doubled, the error between the results is less than 2%). In this paper, two kinds of piston impact bit patterns, the vertical impact of the piston bit and the impact bit after the piston tilt of 0.22° , have been investigated

3 Results

3.1 Carburized layer microstructure and hardness

The internal microstructure of the pistons is shown in Figure 3. Figures 3 (a) and (b) show that the cross-section of carburized layer on the inner and outer surface of the impact piston (see Figure 1.) is acicular martensite. This is due to high carbon content in the carburized layer. When the carbon content is more than 1%wt, the acicular martensite will be formed during quenching. The acicular martensite has the characteristics of high hardness and brittleness^[14]. Figure 3 (c) shows the carburised layer's microstructure at the impact surface (see Figure 1.) of the piston. Comparing the microstructures shown in Figures 3 (a) and (b), it can be found that the microstructure of the impact surface is relatively of fine structure. The piston's internal microstructure shown in Figure 3 (d) is lath martensite and a small amount of lower bainite. As 23CrNi3Mo is the low carbon steel, the quenching microstructure should be lath martensite. However, due to the piston's large size, the quenching cooling process did not result in rapid cooling of the inner part of the piston, explaining the presence of lower bainite. The toughness and plasticity of lath martensite and lower bainite phases are greater than acicular martensite, in contrast to the strength which is lower than the strength of the acicular martensite. In general, the structure of the piston has a hard carburized shell and a softer interior. In the process of impact, the carburized layer cracks easily and leads to piston failure.

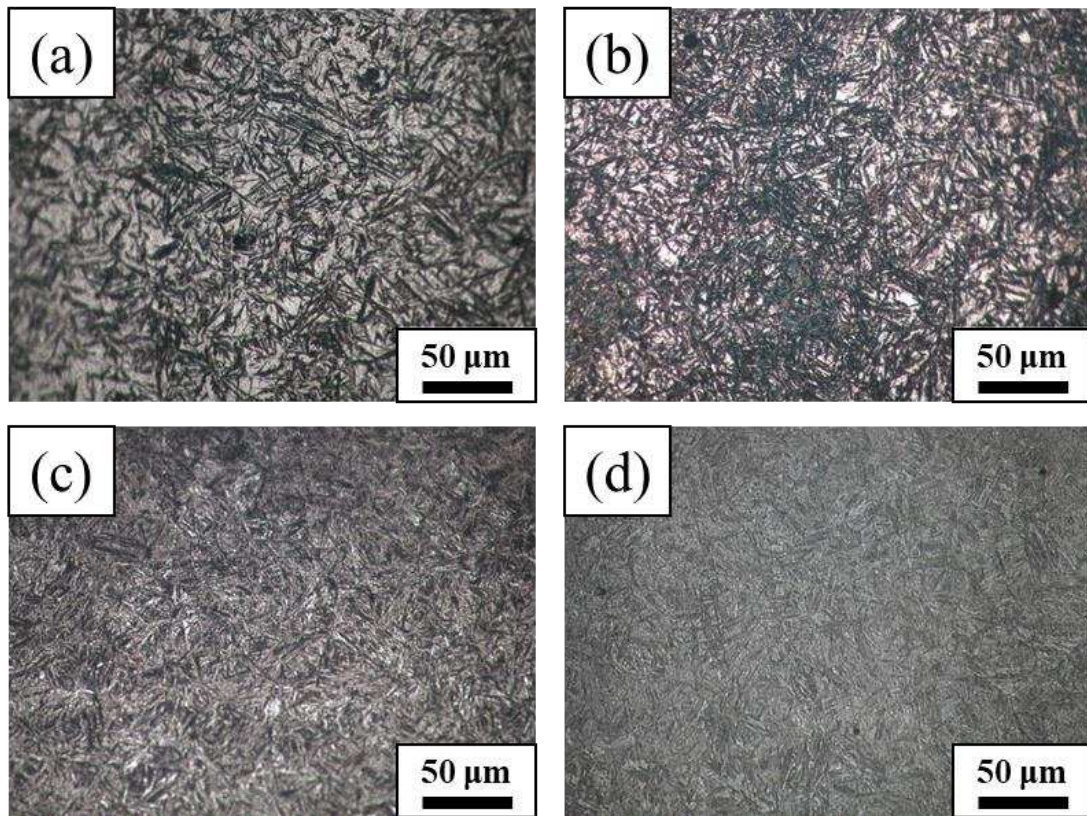


Figure 3 Microstructure of piston at different positions, a) Microstructure of carburized layer on inner surface, b) Microstructure of carburized layer on outer surface, c) Microstructure of carburized layer on impact surface, d) Internal microstructure of piston

The piston's carburized layer is divided into three regions, from the surface to the interior. The observed regions, mainly formed due to different carbon concentration, are characterized with different microstructures and properties (as shown in Figure 4). The first region is within 420 μm from the surface, and its microstructure is acicular martensite due to the highest carbon concentration. The second region is in the range of 420 μm -1300 μm , and this region is mainly a mixed microstructure of acicular martensite and lath martensite. The third region is the internal region of the piston, which is mainly lath martensite and lower bainite. The Vickers hardness gradient of the carburized layer at different piston surface is shown in Figure 4 (b). The hardness decreases gradually with the increased distance from the surface, and finally stabilizes at about 400-500 HV. The hardness of the carburized layer at 2 mm away from the surface is higher than 500 HV, which means that the piston surface hardness meets the production requirements. The hardness of the impact surface is the largest due to the refinement of microstructure and dislocation. Figure 4 (c) shows the detailed hardness gradient by using nano-indentor and its corresponding fracture surface. There are three distinct hardness regions from the surface to the substrate, with the significant transition at a depth of 0.7 mm and 2.1 mm. Corresponding to the fractured section of the surface in Figure 4 (c) (adjusted to the same

scale), the transition points of the hardness shows obvious fracture steps. The hardness distribution of the carburized layer indicates that the hardness is related to microstructure. The outer layer of acicular martensite has the highest hardness, which can improve the wear resistance of piston surface and the steps in the fracture is also related to the change of microstructure accordingly.

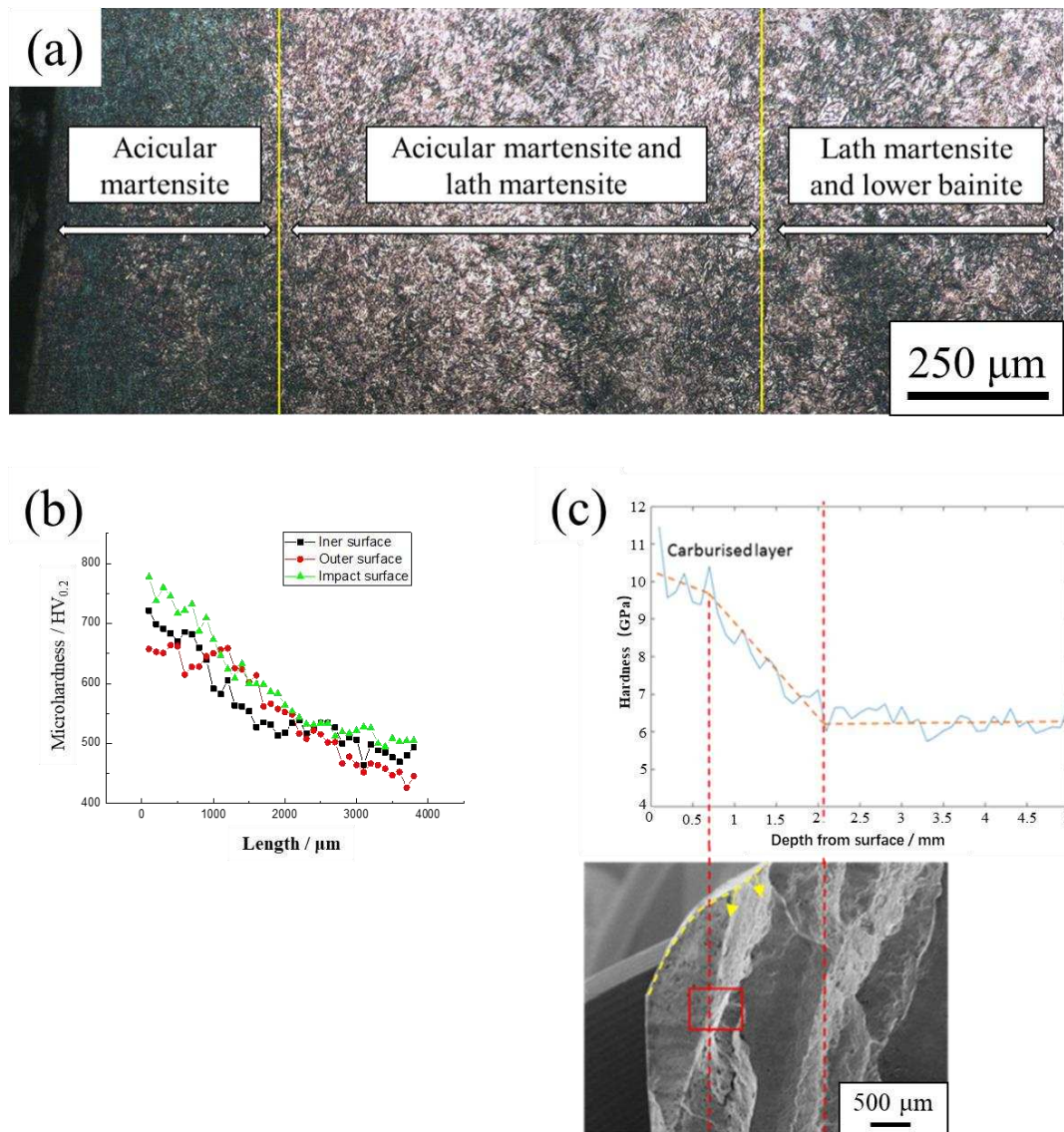


Figure 4 a) Microstructure and b) The Vickers hardness gradient of the carburized layer of piston c) The nano-hardness and the fractured surface

3.2 Carbides in the carburized layer

Prior research has shown that after the carburization of the piston at 850 °C for 10h, carbides may be also be formed in the carburized layer^[10-12]. Figure 5 shows two kinds of carbides precipitated in the carburized layer. The carbide shown in Figure 5 (a) is granular and its size

is between 10-30 μm . According to the composition analysis of EDS, the carbide is mainly composed of iron and carbon. Figure 5 (c) shows a smaller carbide dispersed in the area within 100 μm from the surface. These carbides are mainly composed of carbon and iron. Compared with the carbide shown in Figure 5(a), the carbon content of these carbides is lower. In general, there will be carbides precipitation in carburized layer and these carbides may become the crack sources of piston during impact due to its brittleness. When the distance exceeds 100 μm from the surface, the amount of carbides in the carburized layer is significantly reduced.

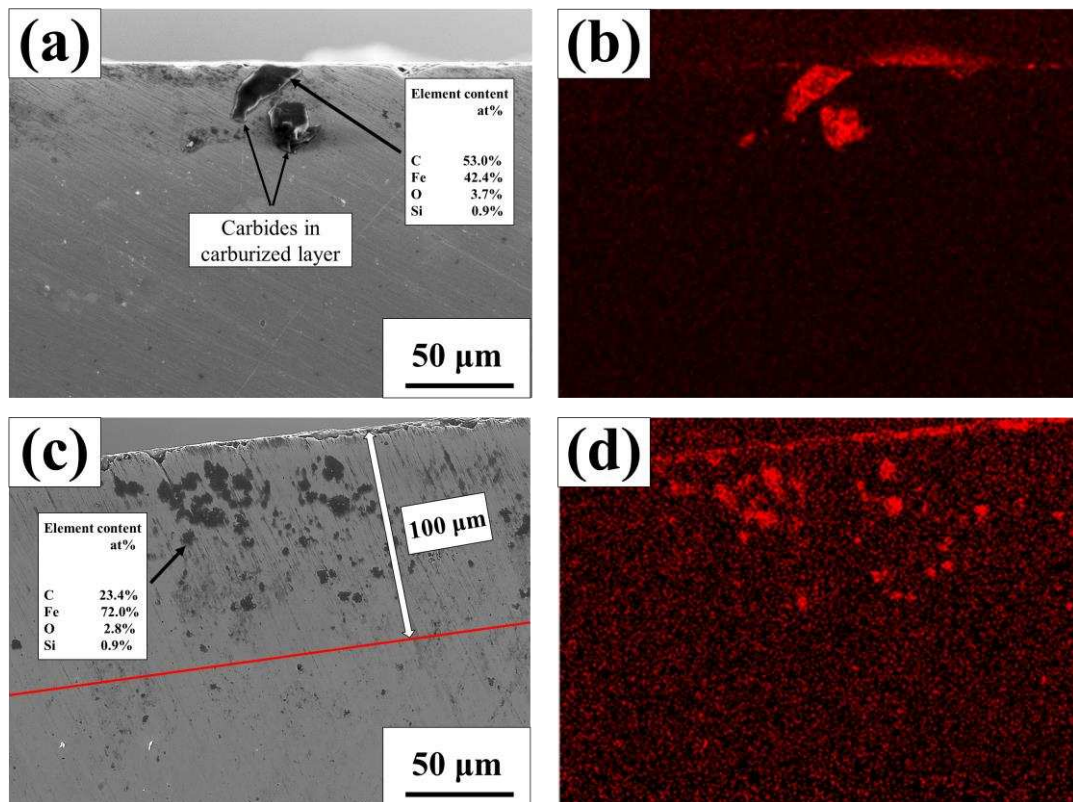


Figure 5 Carbide distribution in the carburized layer, a) Granular carbides and their composition, b) The distribution of carbon element by EDS of Figure 5 (a), c) Dispersed carbides and their composition, d) The distribution of carbon element by EDS of Figure 5 (c)

3.3 Fracture surface morphology

Figure 6 shows the SEM image of the fracture surface located in the red circle in Figure 1 (b). According to the SEM observations in Figure 6(a), with regions A, B and C indicated, the fracture surface of the small cracks is seen to consist of two distinguished regions: the intergranular fracture region A (as shown in Figure 6 (b)) within 430 μm from the surface and the transgranular fracture region C with thickness greater than 430 μm (as shown in Figure 6 (d)). The thickness of the intergranular fracture region is the same as the acicular martensite thickness shown in Figure 4 (a). Therefore, it can be concluded that the intergranular fracture

of the carburized layer is related to the high concentration of carbon in the surface of the carburized layer^[15]. Several researchers have investigated the fatigue fracture mechanisms of carburized steel. It was observed that the cementite formed in the process of carburization accelerates crack propagation along the grain boundaries^[6, 7, 16, 17]. Region B (Figure 6 (c)) shows that there is an apparent boundary between the intergranular fracture region A and transgranular fracture region C. In the transgranular fracture region C, there are obvious river patterns (as shown in Figure 6 (d)). Analysing the river patterns, it can be deduced that the crack propagates from the intergranular fracture region A towards the transgranular fracture region C^[18, 19], so the crack may initiate from the intergranular fracture region A of the carburized layer.

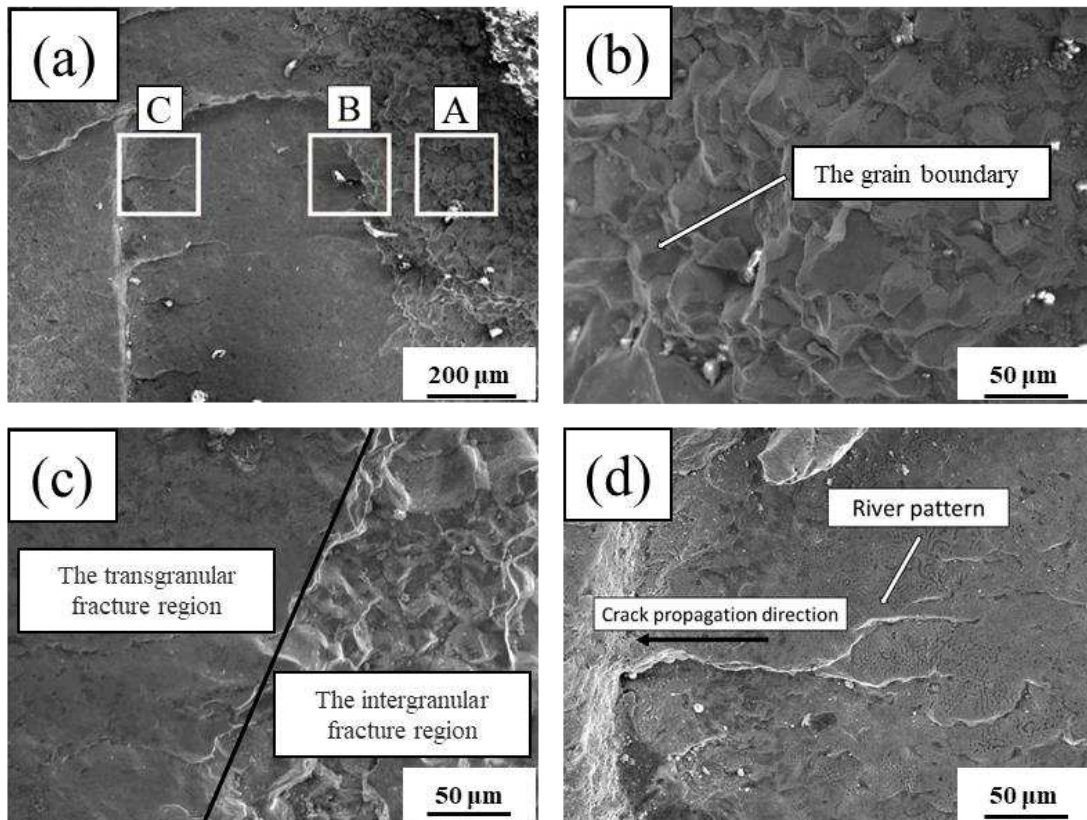


Figure 6 SEM showing the fracture surface of the piston, a) The overall fracture surface, b) The intergranular fracture surface (region A), b) The boundary between intergranular fracture and transgranular fracture (region B), d) The transgranular fracture surface (region C)

3.4 Stress distribution on the impact surface

Figure 7 presents the distribution of von Mises stress and the maximum principal stress on the impact surface when the piston strikes the bit vertically at a speed of 12 m/s. The von Mises stress of the outer and inner edges is larger than that of other regions (as shown in Figure 7(a)). The maximum von Mises stress is located at the outer edge. The value is 520 MPa, which does not exceed the steel's yield strength for the piston. The maximum von Mises stress at the piston's inner edge is 293 MPa, which is lower than that of the outer edge. Compared with the inner edge, the outer edge is more prone to failure when there are defects and inclusions in the material. The maximum principal stresses on the impact surface are shown in Figures 7 (b) and (d). Contrary to Mises stress distribution, the maximum principal stress is distributed at the inner edge of the impact surface. The maximum principal stress of the inner edge is 295 MPa, and that of the outer edge is 31 MPa. Although the maximum principal stress of the inner edge is greater than that of the outer edge, its value is lower than the fatigue limit of the material, so it is difficult to occur fatigue fracture.

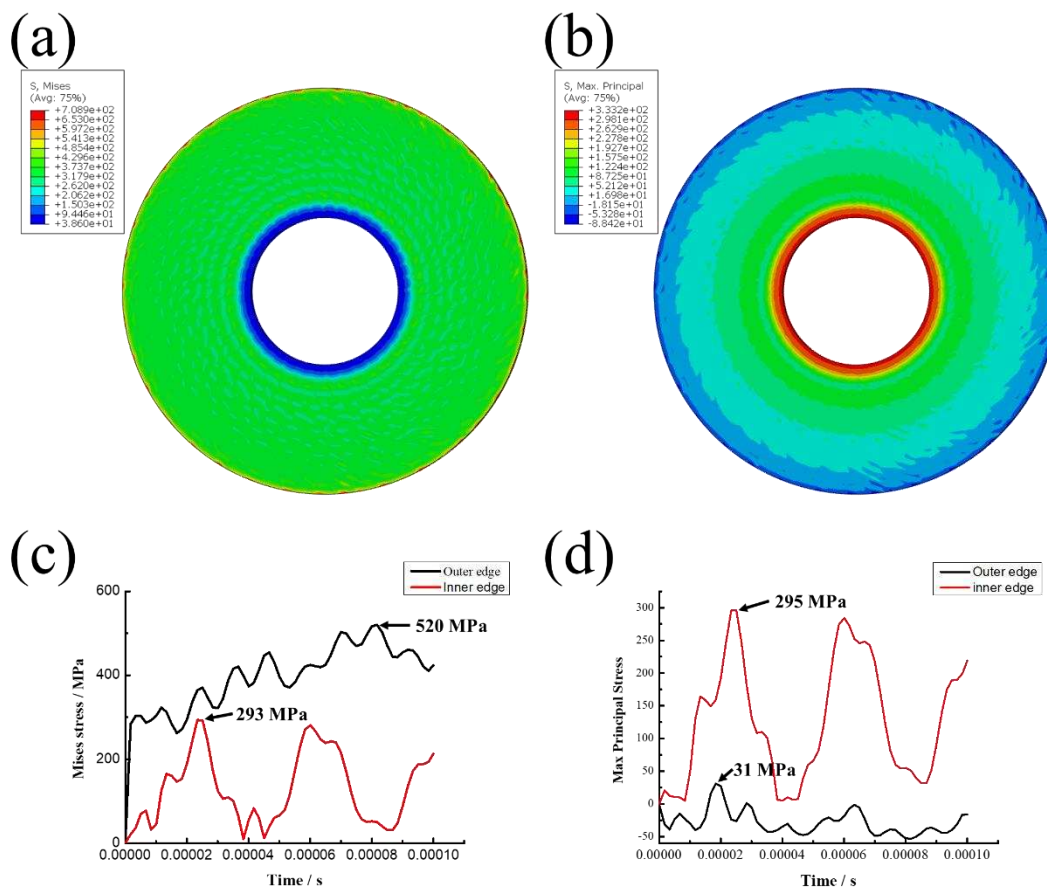


Figure 7 The Mises stress and maximum principal stress distribution, a) The von Mises stress distribution on the impact surface, b) The maximum principal stress distribution on the impact surface,

c) The stress-time curves of outer and inner edge, d) The maximum principal stress-time curves on the outer and inner edge

Due to assembly and wear, there is a gap between the piston of the DTH and the cylinder, which will cause the piston to hit the drill bit obliquely. In this paper, the clearance between the piston and the cylinder is 0.2 mm, and the clearance length is 52 mm, so there is a maximum impact angle $\theta = \arctan \frac{0.2}{52} = 0.22^\circ$ during the impact process. Figure 8 shows the distribution of von Mises stress on the piston impact surface at different times, when the piston strikes the bit at an angle of 0.22° . The von Mises stress increases gradually as it propagates from the impact point to the surrounding. The von Mises stress at the outer edge of the impact surface reaches the maximum value at about 2.66×10^{-6} s, which is 903 MPa (as shown in Figure 8(h)). Compared with the piston vertical impact the drill bit, the von Mises stress value increases by 73%, which means that the damage caused by piston tilting impaction is more serious. The von Mises stress on the inner edge of the impact surface is low during the whole impact process, so the failure probability of the inner edge is lower than that of the outer edge.

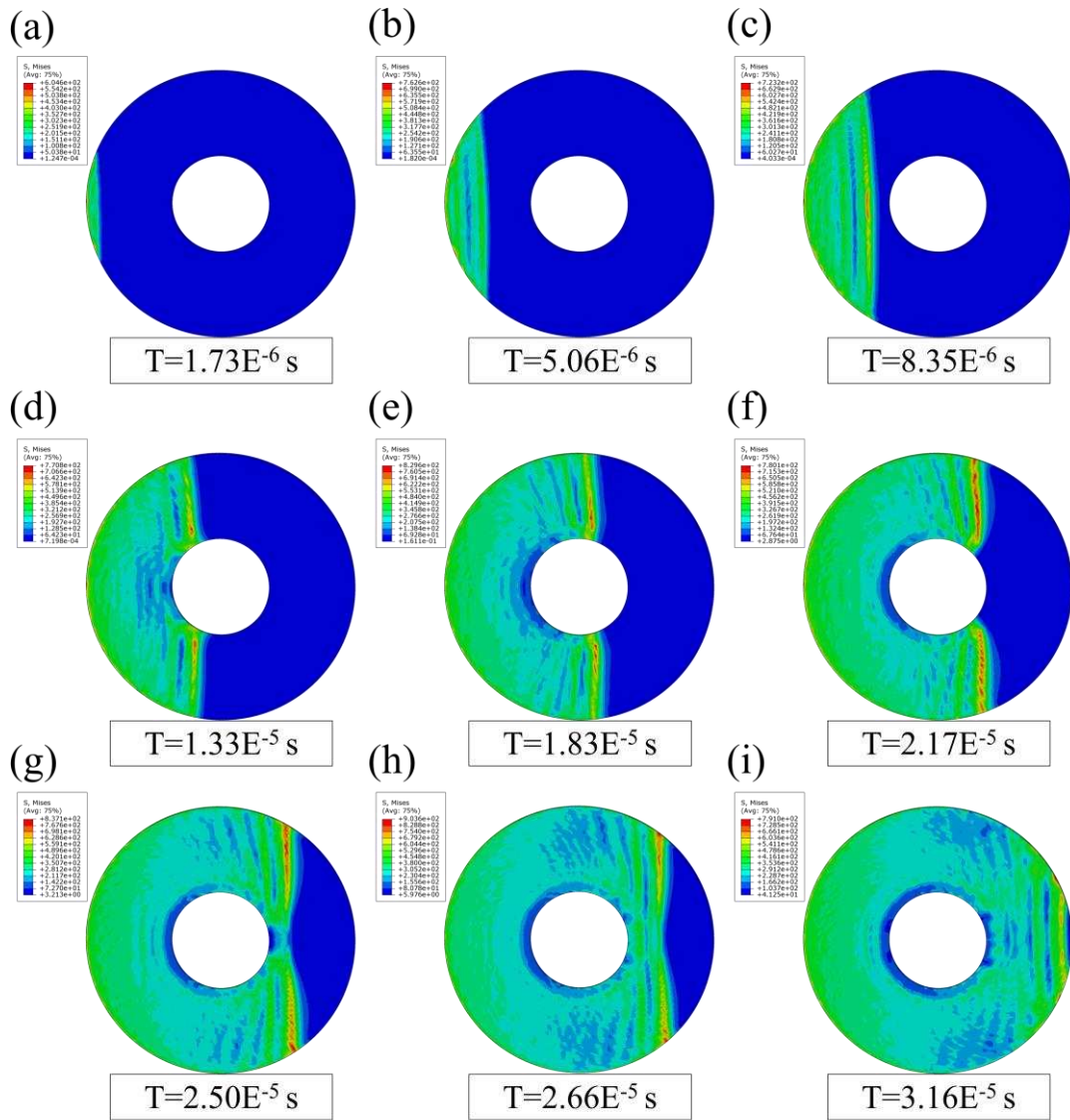


Figure 8 The von Mises stress colour picture of the piston impact surface at a different time when the piston impacts the drill bit at an angle of 0.22°

Figure 9 shows the maximum principal stress colour picture. According to the results in Figure 9 (e), when the piston tilts against the bit, the largest maximum principal stress is located at the inner edge of the piston. Figures 9 (g) and (h) show that the maximum principal stress at the outer edge of the piston is also large during the impact process. The largest maximum principal stress on the outer edge is 560 MPa, which is also higher than that of figure 7 (b).

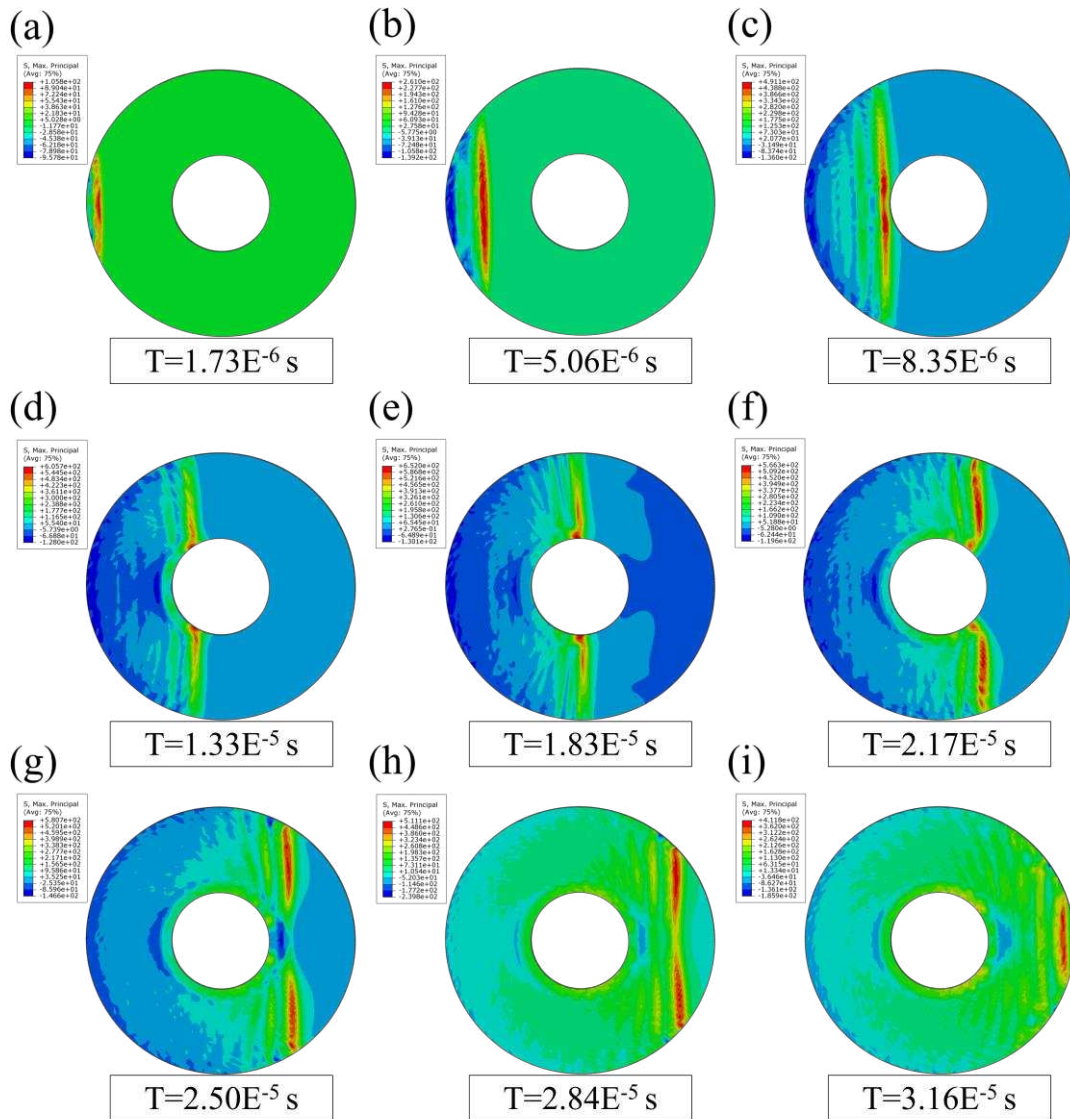


Figure 9 Maximum principal stress colour picture of the piston impact surface at a different time when the piston impacts the drill bit at an angle of 0.22°

3.5 Crack initiation at the outer edge

Figure 10 (a) shows the failed piston's macro small cracks located at the outer edge of the impact surface. These macro small cracks are caused by under the combined action of von Mises stress and maximum tensile stress. Figure 10 (b) and (c) indicate the carbide crack at the outer edge of piston. In the fatigue test of carbon steel, it is proved that carbides in the carburized layer can easily become fatigue source because of their brittleness [13, 20, 21]. In the case of the carburized piston, these carbides are located in the high Mises stress region so they will crack when the piston strikes the bit. Figure 10 (d) point out the maximum principal stress direction and value of the outer edge. The direction of the maximum principal stress is perpendicular to the crack shown in Figure 10 (a), (b) and (c).

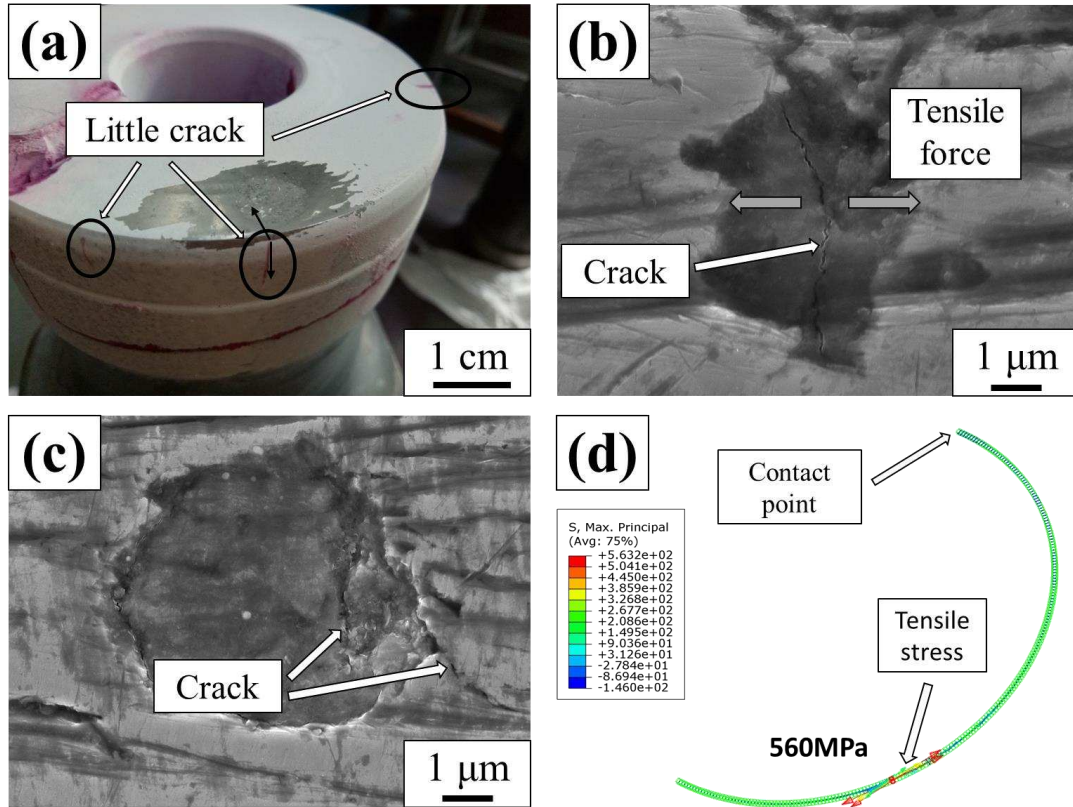


Figure 10 Crack initiation position and stress analysis, a) The crack initiation position and propagation direction, in which the black arrow direction is the crack propagation direction, b) and c) The crack initiated from carbide, d) The direction and value of the maximum principal stress on the outer edge of the piston when hitting the bit at an angle of 0.22°

4 Discussion

4.1 Crack initiation of impact piston

Generally, the uniaxial tensile test or bending fatigue test is used to study carburized steel's fatigue properties [6,7,13,22-24]. The fracture morphology of the impact piston is the same as that of carburized steel. The fatigue sources are located in the carburized layer, and intergranular fracture occurs in the region with high carbon content. But there is a significant difference between the impact piston and the fatigue sample in the stress state. For the impact piston, the stress state of the impact surface is complex. According to the analysis of Figures 7-9, the maximum tensile stress and maximum Mises stress are not located in the same area during the impact. Therefore, it is necessary to explore the role of Mises stress and maximum tensile stress in piston fracture.

According to stress analysis, the Mises stress of the piston impact surface's outer edge is the largest during the impact process. This suggests that the outer edge of the impact end is damaged first, which is consistent with the actual piston failure. From Figure 5 it can be seen

that the outer edge of the piston impact surface will precipitate a large number of carbides during carburizing, and these fragile carbides will crack under the high Mises stress^[25, 26]. After the carbides on the outer edge produce cracks, they will gradually propagate along the direction perpendicular to the tensile stress under the action of tensile stress (as shown in Figure 10).

To further understand the initiation of cracks in the piston, the result of ABAQUS finite element software and Paris' law is used to analyze the fatigue crack initiation on the outer edge of the piston. As mentioned above, the piston's crack propagation direction is perpendicular to the maximum principal stress, so this kind of crack is type I crack. It can be assumed that the initial crack is circular and its direction is subjected to a tensile stress of 560 MPa. The stress intensity factor K can be determined by the following formula^[27]:

$$K = \frac{2\sigma\sqrt{a}}{\sqrt{\pi}} \quad (1)$$

Where a is the crack radius, σ is the tensile stress.

For fatigue cracks, there is a threshold stress intensity factor (ΔK_{th}) for crack growth. When $\Delta K < \Delta K_{th}$, the crack enters the stable growth stage, so this size crack greatly influences the piston failure. Based on Richard's research results^[28], $\Delta K_{th} = E\sqrt{b}$, in which E is the modulus of elasticity, and b is the Burgers vector. According to this formula, the threshold value of piston is $\Delta K_{th}=3.2 \text{ MPa}\sqrt{m}$. The crack diameter can be calculated by introducing K into formula (1)^[28]:

$$a_0 > \frac{\pi\Delta K_{th}^2}{4\sigma^2} \quad (2)$$

According to formula (2), the initial crack size is 51.2 μm which is much larger than the carbide crack size shown in Figure 10. It can be seen from Figure 6 (b) that the fracture mode is intergranular, after crack initiation in the acicular martensite. Due to the precipitation of cementite and carbides at the grain boundary in the region of acicular martensite, fracture toughness is much lower than that in other material regions. Therefore, in the acicular martensitic region, stable crack growth may occur when the crack size is lower than the calculated initial crack size. The length of the acicular martensite region is 430 μm , which is much larger than the initial crack size of the piston. When the crack propagates to acicular martensite boundary, the crack size is much larger than the initial crack size, which means that the crack has entered the stable growth stage.

4.2 Crack propagation of impact piston

The crack propagation is mainly affected by tensile stress and carbides. Figure 11 (a) shows a little crack propagation from the outer edge of the impact surface and this crack splits into *a* and *b* two cracks during propagation process (as shown in Figure 11 (b)). The propagation paths of cracks *a* and *b* are quite different. The crack *a* propagation direction is generally perpendicular to the outer edge of the impact surface. Different from crack *a*, crack *b* gradually changes its direction in the process of propagation, and finally its crack propagation direction is parallel to the direction of tensile stress. The crack propagation direction parallel to the tensile stress will lead to the termination of crack propagation, just like crack *b*, which is also the reason for the different length of crack *a* and crack *b*. As shown in Figure 11 (c), the crack *a* has a sudden change in the propagation direction during the propagation process, which is related to the carbides in the carburized layer of steel. When the crack in Figure 11 (c) propagates to the block carbide, it splits into two cracks along the boundary between the carbide and matrix. One of the cracks can continue to propagate because it is perpendicular to the outer edge, while the other crack stops to propagate because its direction is parallel to the outer edge. In the study of crack propagation, it is also shown that the existence of carbides will affect the crack propagation. The low bonding force between carbide and matrix makes it necessary for crack propagation at carbide boundary^[29, 30]. Beside, the existence of carbides will increase the Mises stress field around it, which makes the area around carbides easy to crack^[31].

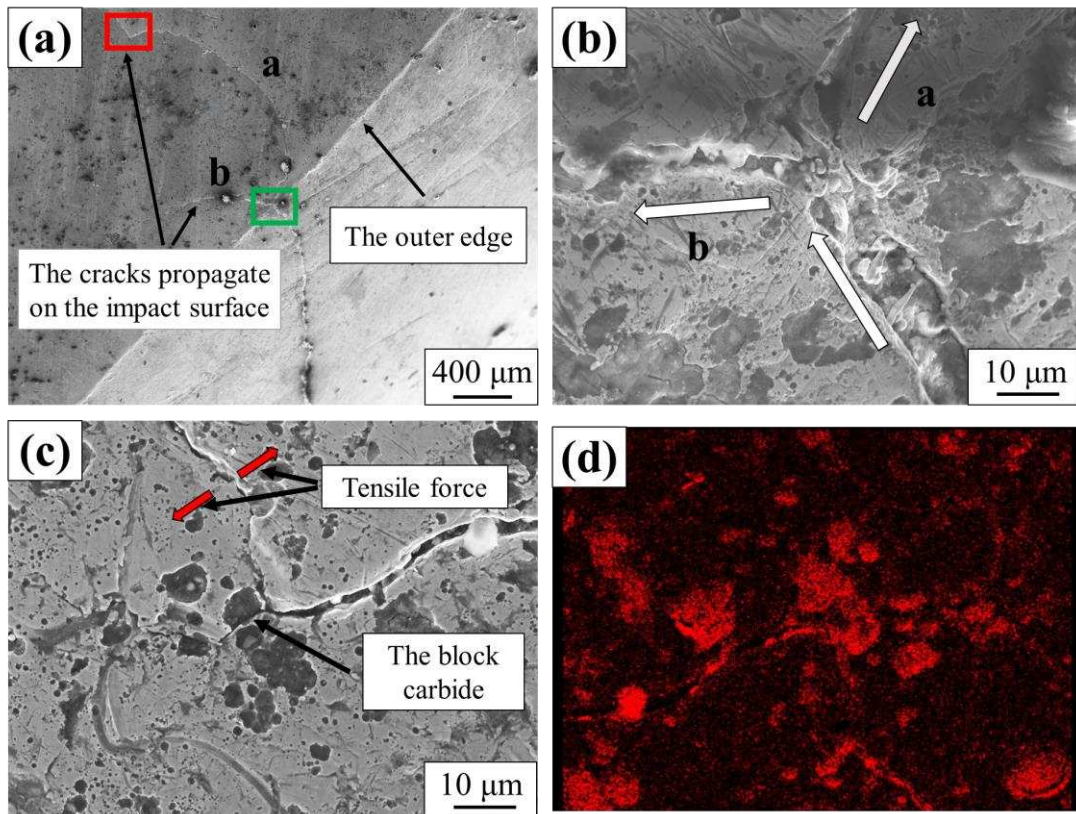


Figure 11 The crack propagates from the outer edge, a) Propagation paths of two cracks *a* and *b*, b) The crack splits into cracks *a* and *b* (Green box in Figure 11 (a)), c) The crack *a* changes its propagation direction (Red box in Figure 11 (a)), d) Figure (c) corresponding carbon EDS

The crack initiation and propagation process of the impact piston is shown in Figure 12. The von Mises stress on the outer edge of the impact end of the piston is relatively high. As there are some brittle carbides in this region, these carbides will crack under the high stress, so the crack initiates at the carbides in the carburized layer. After the crack initiation, it will propagate vertically to the piston because of periodic tensile stress during the impact. In the acicular martensite region, the crack propagates along the grain boundary. When the crack propagates to the acicular martensite boundary, its size is much larger than 51.2 μm and the crack enters the propagation stage. In the plate martensite region of the carburized layer, the fracture mode is an intergranular fracture. In addition to the tensile stress, carbides also affect the crack propagation path. Finally, under the combined action of tensile stress and carbide, the crack propagates along the path with the lowest energy required.

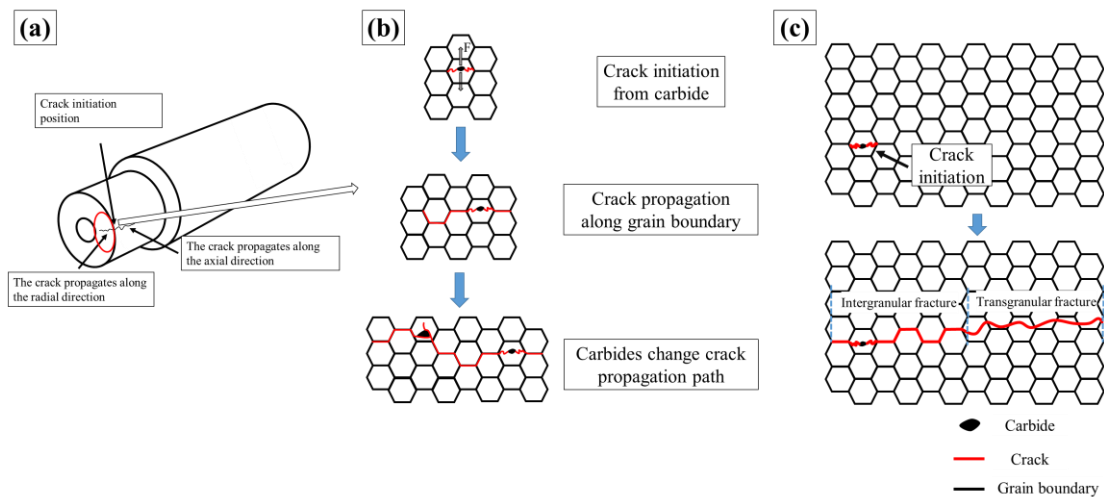


Figure 12 Schematic diagram of crack initiation and propagation, a) Crack initiation and propagation on impact surface, b) The flow chart of crack initiation and propagation mechanism in carburizing layer, c) Flow chart of crack propagation from surface to interior

5 Conclusions

The piston's failure is mainly caused by higher von Mises stress on the outer edge and carbides in the carburized layer. The crack initiation is related to the high Mises stress, and crack propagation is related to the maximum tensile stress. Compared with the piston's vertical impact on the bit, the piston's inclined impact will cause more serious damage to the impact surface. Therefore, the clearance between piston and cylinder should be reduced as far as possible in the process of machining and assembling.

As a weak point, carbides in the carburized layer will crack first during the impact. Many carbides are precipitated in the acicular martensite region, and the size of the acicular martensite region is larger than the initial crack size. Therefore, it is very important to control the carbon potential in the carburizing process to avoid excessive precipitation of large size carbides in the carburized layer. The other key conclusions are:

- The carburizing process will change the microstructure of the piston surface and the microstructure is divided into plate martensite (430 μm), plate martensite + lath martensite (430-1200 μm) and lath martensite structure + lower bainite structure (inside the piston) from the surface to the inside. During the carburization, more carbides are formed in the area within 100 μm near the piston surface.
- In the process of piston impacting the drill bit, the Mises stress is the largest (903 MPa) at the outer edge of the piston. When the piston and the drill bit collide obliquely, the

outer edge of the piston's impact end is subjected to tensile stress and the direction is tangential to the outer edge of the impact end.

- The cracks of the piston initiate from the carbides at the outer edge, which are type I crack. The crack growth is related to the high Mises stress on the outer edge of the piston and the tensile stress during the impact process. Under the effect of tensile stress, the cracks on the outer edge of the plug propagate along the axial and radial direction of the piston.
- When the crack length is more than 51.2 μm , the crack will enter the growth stage from the initiation phase. The crack propagates along the grain boundary in the acicular martensite with high carbon content, and it transforms into transgranular fracture in the lath martensite with low carbon content.

Reference

- [1] T. Sekercioglu, Failure study of pneumatic rock drill piston, *Engineering Failure Analysis* 13(7) (2006) 1108-1115.
- [2] A. Mussa, P. Krakhmalev, J. Bergström, Failure analyses and wear mechanisms of rock drill rods, a case study, *Engineering Failure Analysis* 102 (2019) 69-78.
- [3] J.R. Davis, *Surface hardening of steels: understanding the basics*, ASM international 2002.
- [4] A.J. McEvily, K. Pohl, P. Mayr, Comparison of the fractographic features of a carburized steel fractured under monotonic or cyclic loading, *Materials Characterization* 36(4) (1996) 153-157.
- [5] K.-i. Sugimoto, T. Hojo, Y. Mizuno, Effects of Fine Particle Peening Conditions on the Rotational Bending Fatigue Strength of a Vacuum-Carburized Transformation-Induced Plasticity-Aided Martensitic Steel, *Metallurgical and Materials Transactions A* 49(5) (2018) 1552-1560.
- [6] S. Farfán, C. Rubio-González, T. Cervantes-Hernández, G. Mesmacque, High cycle fatigue, low cycle fatigue and failure modes of a carburized steel, *International Journal of Fatigue* 26(6) (2004) 673-678.
- [7] O. Asi, A.Ç. Can, J. Pineault, M. Belassel, The relationship between case depth and bending fatigue strength of gas carburized SAE 8620 steel, *Surface and Coatings Technology* 201(12) (2007) 5979-5987.
- [8] F. Ernst, Y. Cao, G.M. Michal, A.H. Heuer, Carbide precipitation in austenitic stainless steel carburized at low temperature, *Acta Materialia* 55(6) (2007) 1895-1906.
- [9] F. Ernst, D. Li, H. Kahn, G.M. Michal, A.H. Heuer, The carbide M7C3 in low-temperature-carburized austenitic stainless steel, *Acta Materialia* 59(6) (2011) 2268-2276.
- [10] N.M. Ryzhov, M.Y. Semenov, R.S. Fakhurtdinov, A.E. Smirnov, A model of diffusion growth of carbide-phase particles in the carburized layer of heat-resistant steels, *Metal Science and Heat Treatment* 40(9) (1998) 374-377.
- [11] M.Y. Semenov, Control of heat-resistant steel carburized layer structure. Part I, *Metal Science and Heat Treatment* 55(5) (2013) 257-264.
- [12] M.Y. Semenov, Control of Heat-Resistant Steel Carburized Layer Structure. Part II, *Metal Science and Heat Treatment* 55(5) (2013) 316-321.
- [13] K. Fukaura, Y. Yokoyama, D. Yokoi, N. Tsujii, K. Ono, Fatigue of cold-work tool steels: Effect of heat treatment and carbide morphology on fatigue crack formation, life, and fracture surface observations, *Metallurgical and Materials Transactions A* 35(4) (2004) 1289-1300.
- [14] A. Stormvinter, G. Miyamoto, T. Furuhashi, P. Hedström, A. Borgenstam, Effect of carbon content on variant pairing of martensite in Fe-C alloys, *Acta Materialia* 60(20) (2012) 7265-7274.
- [15] S. Preston, Fatigue Crack Initiation and Growth from a Gas Carburized Surface, *Materials Transactions, JIM* 34(1) (1993) 27-32.

- [16] R.S. Hyde, G. Krauss, D.K. Matlock, Phosphorus and carbon segregation: Effects on fatigue and fracture of gas-carburized modified 4320 steel, *Metallurgical and Materials Transactions A* 25(6) (1994) 1229-1240.
- [17] M.A. Islam, P. Bowen, J.F. Knott, Intergranular fracture on fatigue fracture surface of 2.25Cr-1Mo steel at room temperature in air, *Journal of Materials Engineering and Performance* 14(1) (2005) 28-36.
- [18] K.M. Chang, R. Darolia, H.A. Lipsitt, Cleavage fracture in B2 aluminides, *Acta Metallurgica et Materialia* 40(10) (1992) 2727-2737.
- [19] S. Liu, D. Liu, S. Liu, Transgranular fracture in low temperature brittle fracture of high nitrogen austenitic steel, *Journal of Materials Science* 42(17) (2007) 7514-7519.
- [20] Z. Yong Huang, D. Wagner, Q. Yuan Wang, C. Bathias, Effect of carburizing treatment on the "fish eye" crack growth for a low alloyed chromium steel in very high cycle fatigue, *Materials Science and Engineering: A* 559 (2013) 790-797.
- [21] J. Zhang, R. Prasannavenkatesan, M.M. Shenoy, D.L. McDowell, Modeling fatigue crack nucleation at primary inclusions in carburized and shot-peened martensitic steel, *Engineering Fracture Mechanics* 76(3) (2009) 315-334.
- [22] Na Xiao, Weijun Hui, Yongjian Zhang, Xiaoli Zhao, Ying Chen, Han Dong, High cycle fatigue behavior of a low carbon alloy steel: The influence of vacuum carburizing treatment, *Engineering Failure Analysis*, Volume 109, 2020, 104215, ISSN 1350-6307,
- [23] Yawei Peng, Zhe Liu, Chaoming Chen, Jianming Gong, Marcel A.J. Somers, Effect of low-temperature surface hardening by carburization on the fatigue behavior of AISI 316L austenitic stainless steel, *Materials Science and Engineering: A*, Volume 769, 2020, 138524
- [24] Yong Jiang, Yang Li, Yawei Peng, Jianming Gong, Mechanical properties and cracking behavior of low-temperature gaseous carburized austenitic stainless steel, *Surface and Coatings Technology*, Volume 403, 2020, 126343, ISSN 0257-8972,
- [25] M. Jimenez-Martinez, Manufacturing effects on fatigue strength, *Engineering Failure Analysis* 108 (2020) 104339.
- [26] H. Zhao, G. Wang, H. Wang, Q. Bi, X. Li, Fatigue life analysis of crawler chain link of excavator, *Engineering Failure Analysis* 79 (2017) 737-748.
- [27] P. Paris, F. Erdogan, A critical analysis of crack propagation laws, *Journal of Fluids Engineering, Transactions of the ASME* 85(4) (1963) 528-533.
- [28] R.W. Hertzberg, On the calculation of closure-free fatigue crack propagation data in monolithic metal alloys, *Materials Science and Engineering: A* 190(1) (1995) 25-32.
- [29] W.S. Dai, M. Ma, J.H. Chen, The thermal fatigue behavior and cracking characteristics of hot-rolling material, *Materials Science and Engineering: A* 448(1) (2007) 25-32.
- [30] S.Y. Han, S.Y. Shin, S. Lee, N.J. Kim, J.-H. Kwak, K.-G. Chin, Effect of Carbon Content on Cracking Phenomenon Occurring during Cold Rolling of Three Light-Weight Steel Plates, *Metallurgical and Materials Transactions A* 42(1) (2011) 138-146.
- [31] Jixi Zhang, Rajesh Prasannavenkatesan, Mahesh M. Shenoy, David L. McDowell, Modeling fatigue crack nucleation at primary inclusions in carburized and shot-peened martensitic steel, *Engineering Fracture Mechanics* 76(3) (2009) 315-334